Materials Advances

ROYAL SOCIETY OF CHEMISTRY

PAPER

View Article Online
View Journal | View Issue

Cite this: *Mater. Adv.*, 2026, 7, 4226

Multi-resonant thermally-activated delayed fluorescence (MR-TADF) emitters for blue organic light-emitting transistors (OLETs)

Georgios Fanourakis, *[a] Amirhossein Azari [a] and Caterina Soldano *[ab]

Received 10th December 2025,
Accepted 24th March 2026

DOI: 10.1039/d5ma01444a

rsc.li/materials-advances

Thermally-activated delayed fluorescence (TADF) molecules are a promising class of emitters for organic optoelectronic devices, potentially more efficient than phosphorescent emitters. Among them, multi-resonant TADF (MR-TADF) emitters are designed to enhance the rigid molecular structure, leading to a narrow-band emission below 50 nm. In this work, we studied a multi-resonant TADF material, *t*-DABNA, embedded in DPEPO as a blue emissive layer in organic light-emitting transistors (OLETs), a device platform that combines into a single device the switching capability of a transistor and the light emission of an organic light-emitting diode. We investigated the effect of different *t*-DABNA concentrations within the emissive blend in a multilayer heterostructure, and we analyzed our experimental results in terms of optical, morphological, and optoelectronic properties of the blend itself. We found that emitter content of approximately 10% leads to the highest external quantum efficiency (0.18%) in the devices and with a narrow band emission as low as 30 nm. This work offers key insights into the use of MR-TADF emitter molecules within organic field-effect light-emitting devices.

Introduction

Organic light-emitting transistors (OLETs) are multifunctional optoelectronic devices that integrate into a single device the switching capability of a transistor and the light emission of a light-emitting diode.[1–5] In 2003, Hepp *et al.* showed that a single thin-film layer tetracene transistor exhibited light emission in the visible spectrum,[6] thus opening the way to more detailed and extended studies on this optoelectronic device platform.[7–9]

Achieving high performance OLET with a single material requires the active organic layer to have both high charge carrier mobility and emission efficiency; however, these characteristics are unlikely present at the same time in a single material as high mobility relies on dense molecular packing, whereas such packing often leads to aggregation-induced quenching (AIQ) of the emission.[10,11] In this regard, multilayer heterostructures (two or more layers) have been proposed to spatially separate the region where transport occurs from the one where light is generated, leading to an overall improvement of the external quantum efficiency (EQE) of the device.[12] Organic light-emitting transistors rely mostly on lateral transport and charge injection at the organic-metal interface, so achieving balanced electron and hole transport towards the emission layer, especially in a multilayer heterostructures, is non-trivial and strongly depending on the contact geometry and configuration, energy alignment of both highest occupied molecular orbital (HOMO) and lowest unoccupied molecular orbital (LUMO) of the materials stack, layer morphology and semiconductor properties.[13]

Multilayer OLETs with holes and electrons transported independently through different layers towards the emissive layer (where radiative recombination occurs) have demonstrated superior efficiency compared to their diode counterpart, when using the same set of materials.[14] Decoupling exciton formation and decay from charge transport allows for independent use and optimization of high-mobility organic materials and highly efficient emitters. Emissive layer typically consists of a host–guest system (blend), where the host favours charge or energy transfer to the emitter molecules (responsible for the light emission), while at the same time spatially separating them to prevent exciton–exciton quenching phenomena.[15–17] To favour exciton formation and energy transfer, the triplet energy level of the host should be higher than the triplet energy level of the emitter.[18,19] While on one side low emitter concentrations result in low emission, on the other hand, high guest concentrations often lead to quenching phenomena such as aggregation-induced quenching and the formation of

[a] *Department of Electronics and Nanoengineering, School of Electrical Engineering, Aalto University, 02150 Espoo, Finland. E-mail: georgios.fanourakis@aalto.fi, caterina.soldano@aalto.fi*
[b] *Quantum Materials and Sensing Institute, Northeastern University, Burlington, MA, 01803, USA*

non-radiative paths.[17,20] Thus, the optical properties of the blend (*i.e.*, guest content and dispersion) are key for colour purity of the device and, to some extent the overall device efficiency.[21–24]

Among many emitters, thermally-activated delayed fluorescent (TADF) molecules have arisen as a promising class of luminescent materials able to potentially achieve 100% internal quantum efficiency.[25,26] TADF molecules are designed such that thermal energy can enable reverse intersystem crossing (rISC) between triplet (T_1) and singlet state (S_1). For this process to occur, the energy difference ΔE_{ST} between the first excited singlet and triplet needs to be small (<0.2 eV).[27–29] This can be achieved by implementing a donor acceptor (D–A) molecular structure[30–33] which leads to a reduced exchange integral (J) between the HOMO and the LUMO of the emitter. While TADF molecules can lead to efficient light generation processes in organic devices, they still exhibit a relatively wide emission spectrum (>70 nm)[34] due to strong charge transfer excited states and the non-rigid structure that leads to vibrational coupling of the excitons with the molecule.[35] In this scenario, multi-resonant TADF (MR-TADF) emitters have been recently proposed; they strategically incorporate atoms with opposing resonance effects (*i.e.*, combination of an electron deficient boron (B) atom and an electron rich nitrogen (N) atom into a more rigid, planar structure[36–38]), which localize HOMO and LUMO orbitals on different atoms of the molecule, favouring energetically closer singlets and triplets. The first demonstration of this class of emitters was reported by Hatakeyama *et al.* with DABNA-1 and DABNA-2, which combine nitrogen and boron atoms in a para-arrangement with a rigid triphenylborane-based π-core, enabling multi-resonant effect.[39] This led to an intrinsic narrow band emission spectrum[40,41] in comparison to phosphorescent emitters and conventional D–A TADF,[39,42] with an overall full-width at half maximum (FWHM) below 50 nm.[43]

Maintaining narrow emission and high quantum yield in solid-state films represents a major challenge in MR-TADF emitters blends as spectral broadening due to the strong π–π interactions can occur even at low concentrations.[44] Modifying the molecular structure of the emitter with additional groups, such as *tert*-butyl, enhances the steric hinderance thus reduces the close packing between emitters, suppressing excimer formation[45–47] that can decrease emission efficiency. In this context, *t*-DABNA is a MR-TADF emitter with four bulky *tert*-butyl groups surrounding the core structure which exhibit high photoluminescence quantum yield (PLQY), when doped in DPEPO even at relatively high concentrations (10 wt%).[48]

Recently, MR-TADF emitters integrated in lateral OLET architectures combined with intrinsic multiple-order microcavities, have shown EQE values of 5.9% with a FWHM of 13 nm for *t*-DABNA (in mCBP host).[49] However, systematic investigation of MR-TADF host–guest blends under field-effect operation, and particularly the role of guest concertation on optical, morphological, and device properties remain limited.

Here, we fabricated and study the optoelectronic properties of organic light-emitting transistors where the active region is composed of a *p*-type semiconductor layer 2,7-dioctyl[1]-benzothieno[3,2-b][1]benzothiophene (C8-BTBT) in direct contact with the dielectric and an emissive layer consisting of bis[2-(diphenylphosphino)phenyl] ether oxide DPEPO (host) and 2,12-di-*tert*-butyl-5,9-bis(4-(*tert*-butyl)phenyl)-5,9-dihydro-5,9-diaza-13b-boranaphtho[3,2,1-de]anthracene *t*-DABNA (MR-TADF guest). We selected DPEPO as the host material based on several considerations: (i) large HOMO–LUMO gap (4.1 eV) particularly suitable for hosting blue emitters, (ii) electron-transporting hosts can improve charge balance in field-effect devices[50] while also complementing our hole-transporting *p*-type dominated device architecture, (iii) DPEPO's high triplet energy (T_1 = 3 eV) exceeds that of *t*-DABNA, which is essential for confining triplet excitons on the emitter and enabling efficient reverse intersystem crossing. We systematically investigated the influence of *t*-DABNA guest concentration within the emissive blend in terms of optical properties, morphological and optoelectronic properties on the overall device performance. This study offers key insights into the role of MR-TADF emitter molecules within organic field-effect devices and establishes composition guidelines for optimizing narrowband-emitting OLETs.

Experimental section

Glass substrates with pre-patterned indium tin oxide (ITO) were first cleaned with deionized water (DI) water with diluted Hellmanex III (Ossila), then rinsed with DI water, followed by sonication first in acetone and then in isopropanol. The DI water step lasted for 5 minutes, and all the others lasted 10 minutes. Oxygen plasma treatment (100 Watt for 15 minutes) was used to enhance the hydrophilicity of the sample's surface. Immediately after the surface plasma treatment, 400 nm of poly(methyl-methacrylate) (PMMA), (Allresist AR-P 679.04) was deposited on the substrates by spin-coating and annealed on a hot plate at 110 °C for 30 minutes in ambient conditions. After that, the samples were loaded in the evaporation chamber (Moorfield Nanotechnology MiniLab90) for device fabrication, including deposition of the organic semiconductor (C8-BTBT, Sigma Aldrich, 30 nm) in direct contact with the dielectric surface and the emissive blend (60 nm) composed of the host DPEPO and different guest *t*-DABNA content (both materials from Ossila). Then, we deposited silver electrodes (70 nm) on top of the emissive blend, which will act as the source and drain. All depositions were carried out at a base pressure of 10^{-7} mbar with shadow masks to create the device geometry (same channel width and length for all devices). All thicknesses were measured with a stylus Dektak/XT profilometer. The electrical characterization was performed inside a glovebox under N_2 atmosphere at room temperature. A semiconductor device analyzer B1500A Keysight equipped with a Hamamatsu S1337 photodiode was implemented for optoelectronic characterization. The photodiode is placed in contact with the back side of the substrate using a custom-built set-up, thus enabling the measurement of the bottom emission (light emitted through the bottom gate and the substrate). The

electroluminescence (EL) spectra were acquired using a Konica Minolta CS-2000 spectroradiometer. The surface morphology was studied with a Bruker Dimension Icon atomic force microscope (AFM) with a scan size of 10 μm × 10 μm and 256 lines/scan resolution. Photoluminescence (PL) measurements were carried out with a homemade setup utilizing a He–Cd laser system with excitation wavelength at 325 nm.

Results and discussion

DPEPO:*t*-DABNA blends under optical excitation

Fig. 1a shows the normalized PL spectra for DPEPO:*t*-DABNA emissive blends (60 nm) deposited on Si/SiO_2 substrates with guest concentrations of 5, 10, 15 and 20% (as labelled). The spectrum of a neat *t*-DABNA film (30 nm) is also included as reference. Independently of *t*-DABNA content within the blend, all photoluminescence spectra exhibit almost a full overlap for wavelengths up to 500 nm, with main peak around 470 nm and values of FWHM of approximately 40 nm. The origin of narrow emission is briefly described in Supplementary Information (Fig. S1). At higher wavelengths ($520 < \lambda < 600$ nm), we observed the excimer contribution with increasing *t*-DABNA concentration within the blend, commonly observed in host–guest systems with increasing guest content.[44,51] In the case of neat *t*-DABNA film (dashed line), the main excitonic peak

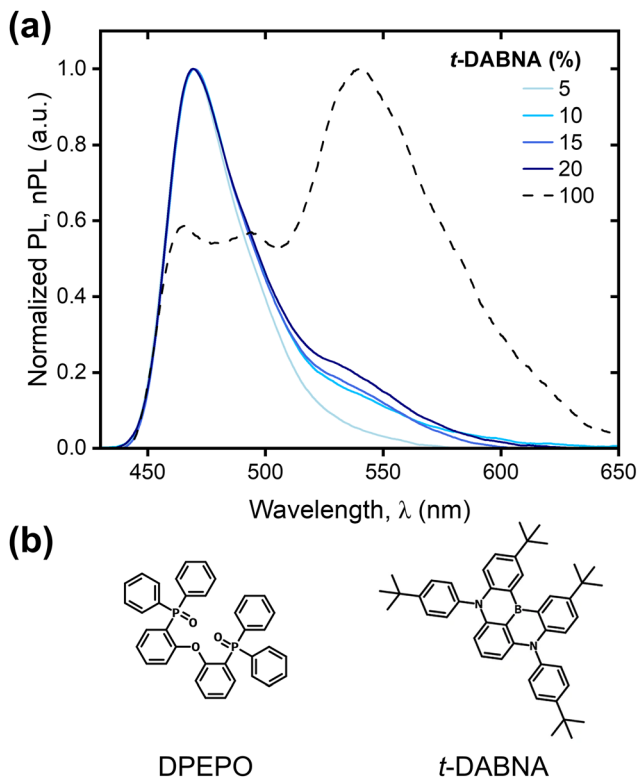

Fig. 1 (a) Room temperature normalized photoluminescence (nPL) of DPEPO:*t*-DABNA blends deposited on Si/SiO_2 for different *t*-DABNA content within the blend (as labelled). Normalized photoluminescence (dashed line) of a neat film *t*-DABNA is also reported as reference. (b) Chemical structures of DPEPO and *t*-DABNA.

(~465 nm) is quenched and the broadening of the peak at lower energies becomes dominant. There is a small redshift of the main excitonic peak of neat *t*-DABNA and the DPEPO:*t*-DABNA blends (~5 nm), possibly due to the polarity of the host.[52] The peak position and the FWHM of the PL are summarized in Table T1 (SI). We note that the emission intensity of *t*-DABNA neat film for wavelengths above 500 nm is larger compared to those coming from the blends (Fig. S2, Supporting Information). DPEPO neat film shows no detectable PL under 325 nm excitation (not shown), demonstrating that the observed emission arises entirely from *t*-DABNA. Fig. 1b shows the chemical structures of the host (DPEPO) and guest (*t*-DABNA). DPEPO is a phosphine oxide-based material ideal for hosting blue organic dyes due to its large HOMO–LUMO gap (4.1 eV) and high triplet energy $T_1 = 3$ eV;[53] on the other hand, *t*-DABNA, is a highly rigid multi-resonant thermally-activated delayed fluorescence emitter with four bulky *tert*-butyl groups that enhance the steric hindrance and mitigate aggregation and π–π stacking between adjacent emitter molecules providing high efficiency even at relatively high doping concentrations.[39,43] The photophysical properties of *t*-DABNA have been investigated in different hosts, including 3,3′-di(9*H*-carbazol-9-yl)-1,1′-biphenyl (mCBP) and DPEPO and it has been shown to exhibit a FWHM smaller than <40 nm,[49,54,55] which is consistent with our experimental findings. Further, PLQY of approximately 75% has been found for *t*-DABNA in DPEPO at 10% doping concentrations,[48] suggesting that *t*-DABNA retains high emission efficiency within DPEPO at these doping contents.

Organic light-emitting transistors with DPEPO:*t*-DABNA blends

Fig. 2a illustrates (top) a schematic representation of our device and (bottom) the corresponding energy levels for the organic materials. Upon biasing the device, electrons are injected from the drain into the emissive layer, while holes are injected from the source and transported towards the *p*-type layer by the strong vertical electric field. Electrons tend to accumulate in the emissive layer near the drain electrode while holes are transported from the source to the drain horizontally through C8-BTBT. Given the lower triplet energy of *t*-DABNA with respect to DPEPO,[48,53] light emission will occur on *t*-DABNA as electrons and holes will occupy the LUMO and HOMO of *t*-DABNA prior to recombination (Fig. 2a bottom). Fig. 2b shows the saturation transfer curves (I_{ds} *vs.* V_{gs} at $V_{ds} = -100$ V) of representative organic light-emitting transistors with different DPEPO:*t*-DABNA emissive blends (as labelled). We measured at least six devices for each configuration. As expected, charge transport in all organic light-emitting transistors is dominated by holes, with similar values of drain-source currents at the highest applied bias ($V_{ds} = V_{gs} = -100$ V). Electroluminescence (EL) is reported on the right *y*-axis, and both *x*- and *y*-axes are kept the same in all panels to favour a direct comparison among different devices.

The drain-source current in saturation regime in a unipolar transistor can be written as follows:

$$I_{ds,sat} = \frac{W}{2L}\mu_{sat}C_i\left(V_{gs} - V_{th}\right)^2 \quad (1)$$

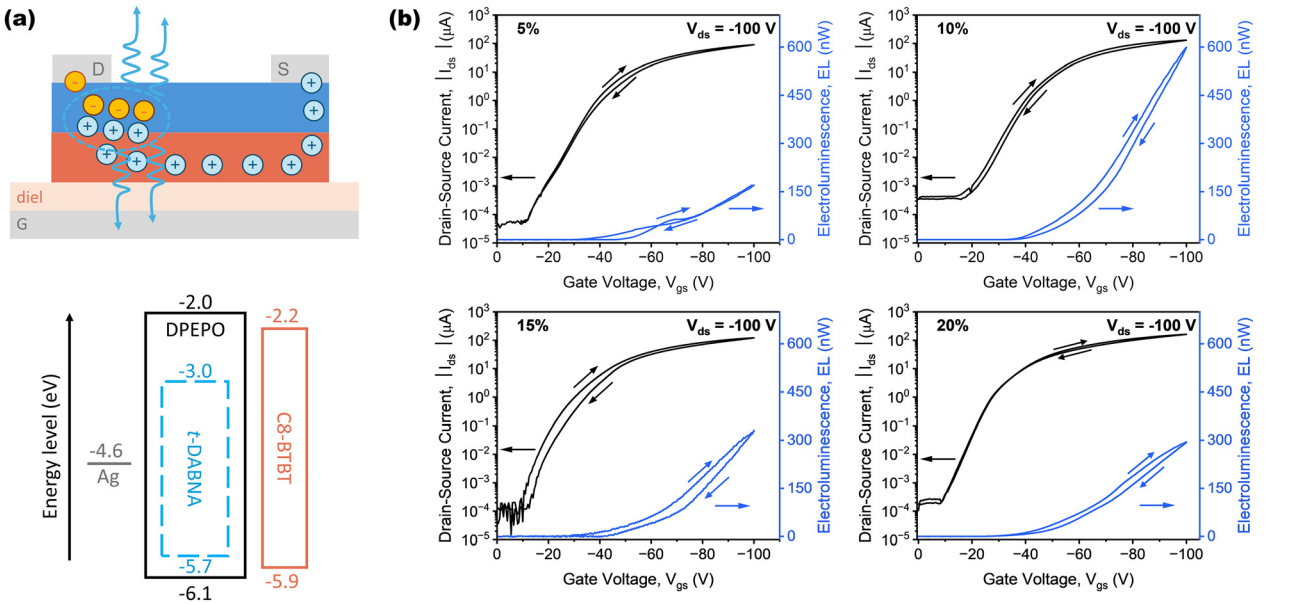

Fig. 2 (a) Schematic representation of (top panel) bi-layer organic light-emitting transistor and (bottom panel) corresponding energy diagram. (b) Saturation transfer curves (I_{ds} *vs.* V_{gs} at V_{ds} = −100 V) for OLET with different emitter content in the emissive layer 5, 10, 15 and 20% (as labelled). Right *y*-axis reports the light generated in the device and measured through the gate (bottom emission). Direction of the sweeps is also indicated.

Table 1 Summary of optoelectronic properties of organic light-emitting transistors with DPEPO:*t*-DABNA emissive layers with different *t*-DABNA content

t-DABNA content (%)	Saturation mobility, μ_{sat} ($cm^2\ V^{-1}\ s^{-1}$)	Threshold voltage, V_{th} (V)	ON/OFF ($\times 10^5$)	EQE (%)	EL peak (nm)	EL FWHM (nm)
5	0.15 ± 0.04	−33 ± 3	21.9	0.06	466	30
10	0.24 ± 0.03	−38 ± 4	3.8	0.18	468	30
15	0.23 ± 0.04	−28 ± 4	9.3	0.11	469	39
20	0.19 ± 0.04	−26 ± 2	15.5	0.06	468	37

where W and L represent the channel width (W = 5 mm) and length (L = 100 μm), C_i the capacitance per unit area of the dielectric (C_i = 6.6 nF cm^{-2} for PMMA[21]), μ_{sat} the saturation mobility and V_{th} the threshold voltage of the transistor. Table 1 summarizes the figures of merit for our organic light-emitting transistors, with values of field-effect saturation mobility and threshold voltage derived from the saturation transfer curves.[56] All our transistors exhibited similar saturation mobility values in the range 0.15–0.24 $cm^2\ V^{-1}\ s^{-1}$, and values of threshold voltages between −38 V and −26 V, with seemingly no dependence on the guest content within the emissive blend. These results are also consistent with some of our previous studies using phosphorescent molecules in emissive blends.[23] All devices exhibited an ON/OFF ratio in the range of 10^5, with differences mainly arising from different OFF-state currents (gate leakage current). We note here that all our transistors show negligible hysteresis.

While our experimental results do not show major differences in purely electronic properties, in terms of light generated in the device (and measured through the bottom gate), we observed variations depending on the *t*-DABNA content within the blend, with the highest EL value for DPEPO:*t*-DABNA 10% (Fig. 2b). Fig. 3a shows the EQE (ratio between the emitted optical power and the charge carriers injected into the device) as a function of the *t*-DABNA content within the emissive blend. We found that the organic light-emitting transistors using the emissive blend containing 10% *t*-DABNA are the most efficient devices, with approximately two times higher efficiency compared to the other devices. This dependence is rather expected in host–guest emissive blends,[23,24] where at low concentration of emitters, the average distance between a host and a guest molecule is larger than the energy transfer radius leading to excitons that are created in the host to decay non-radiatively.[57] On the other hand, at higher emitter loads, guest molecules are in close proximity, this enhances non-radiative recombinations, causing concentration quenching and excimer formation that have a negative effect on emission efficiency.[17,58,59] Further, we found that the values of external quantum efficiency remain approximately constant as a function of bias in the saturation regime (Fig. S3a, SI). Fig. 3b shows the optical image of one of our representative OLET device (emissive blend: DPEPO:*t*-DABNA 10%) in its ON-state (V_{ds} = V_{gs} = −100 V), as viewed through the bottom gate electrode (bottom emission).

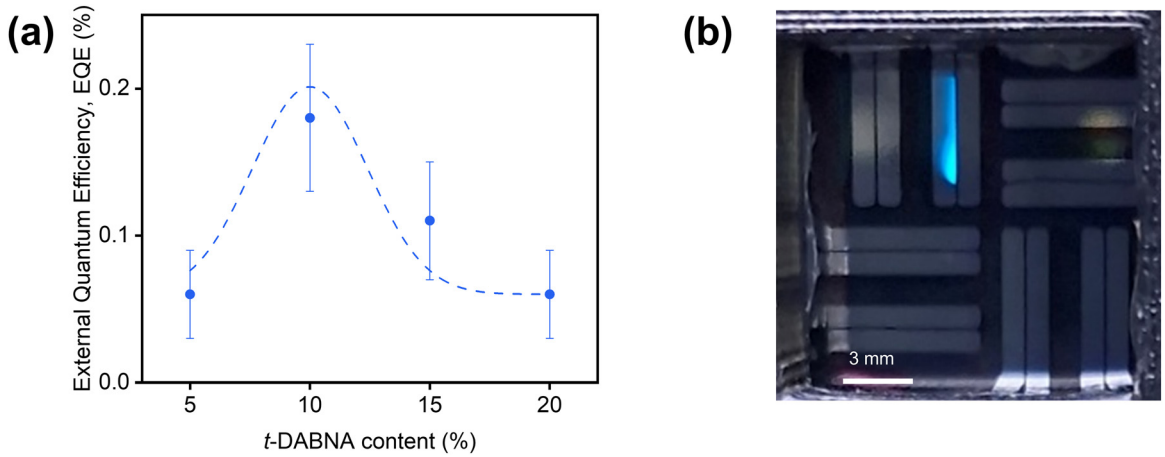

Fig. 3 (a) External quantum efficiency of our organic light-emitting transistors as function of the *t*-DABNA content within the blend. Dashed line is a *guide-to-the-eye* only. (b) Optical image of a bilayer OLET using DPEPO:*t*-DABNA 10% as emissive blend in its ON-state (V_{ds} = V_{gs} = −100 V).

The light emission occurs near the edge and under the drain electrode, due to the unipolar nature of charge transport in our device.

Variations in molecular packing and surface morphology can lead to changes in the injection mechanism, thus potentially affecting the optoelectronic properties of the devices.[60]

Fig. 4 shows the surface morphology of our emissive layers within the device channel as studied by atomic force microscopy (AFM). We observed that all blends exhibit very similar morphology with generally smooth surfaces (root mean square roughness, rms of approximately 4–5 nm), with the blend growth retracing the underlying C8-BTBT surface.

This is also consistent with some of our previous work, using different emissive blends.[22–24] AFM image of the underlying *p*-type surface layer (on PMMA) is reported in Fig. S4 (SI) as a reference. Fig. 4 shows no correlation between surface morphology and the *t*-DABNA content within the emissive blend, suggesting that the contribution to charge injection, and possible contact resistance, is expectedly the same for all devices. Thus, our experimental results on optoelectronic properties of our light-emitting transistors (Fig. 2) along with the morphology information (Fig. 4) suggest that the improved efficiency of the device using the blend DPEPO:*t*-DABNA 10% (Fig. 3) is more likely related to the intrinsic photophysical properties of the blend itself.

Fig. 5a shows the normalized electroluminescent spectra for our organic light-emitting transistors using emissive blends with different *t*-DABNA content (as labelled). Similarly to our results in the case of optical excitation (Fig. 1), all spectra exhibit a dominant emission peak at around 468 ± 3 nm, which is independent of the content of *t*-DABNA within the blend and a broadening of the spectra with increasing concentration. All devices present a FWHM below 40 nm, with 5% and 10% DPEPO:*t*-DABNA OLETs exhibiting a FWHM as low as 30 nm, which is smaller than the FWHM reported in organic light-emitting transistors with phosphorescent[61] and TADF emitters.[22,24,62–64] For increasing *t*-DABNA concentrations (15 and 20%) within the blend, we observed an overall broadening of the electroluminescent spectra. Colour coordinates of our devices are reported in Table T2 (SI), along with their placement on the Commission Internationale d'Eclairage (CIE) 1931 diagram (Fig. S3b, SI). Fig. 5b shows the dependence of the electroluminescence spectrum) from the applied bias (V_{gs} = V_{ds} as labelled) for our organic light-emitting transistor (DPEPO:*t*-DABNA 10% emissive blend). We observed an increase in the amplitude of the electroluminescence with increasing applied bias, while the position of the main emission peak and its width remained unchanged, as shown in the inset. In addition to efficiency and spectral purity, operational and spectral stability under electrical bias are key requirements

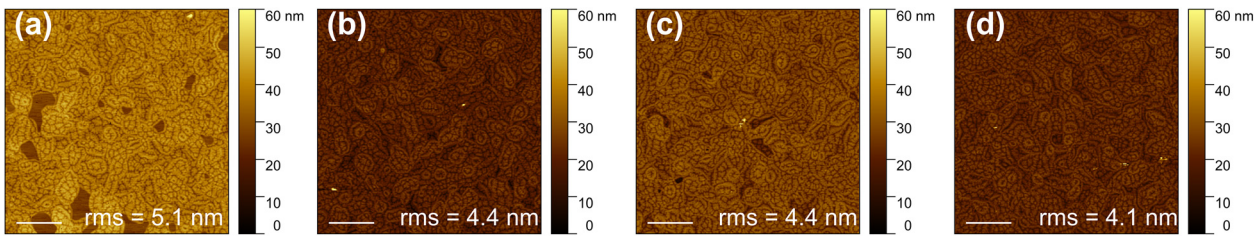

Fig. 4 Atomic force microscopy (AFM) micrographs of emissive blends with different *t*-DABNA content as deposited on C8-BTBT: (a) 5, (b) 10, (c) 15 and (d) 20%. Values of surface roughness are also reported in the bottom right corner. Image size 10 μm × 10 μm and scale bar is 2 μm for all micrographs.

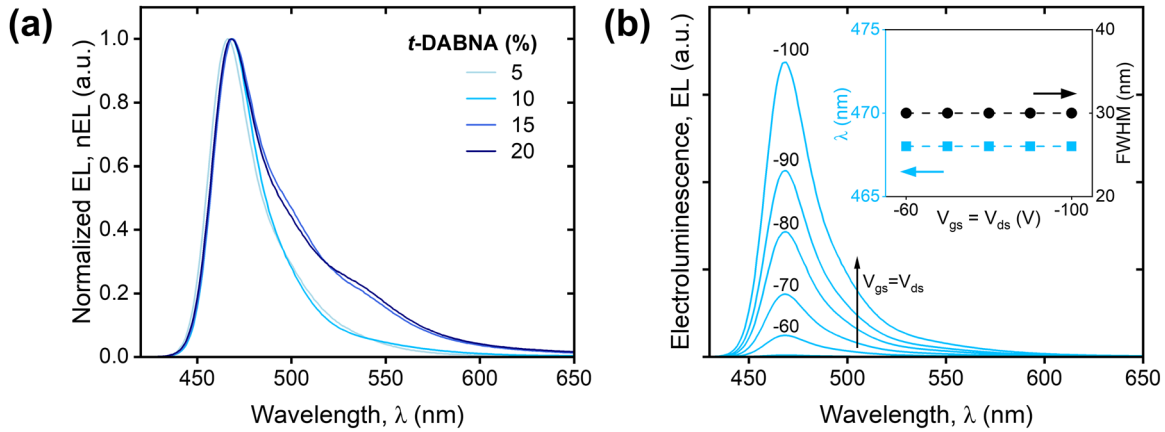

Fig. 5 (a) Normalized electroluminescence for OLET using different DPEPO:t-DABNA emissive layer (as labelled). (b) Electroluminescence spectrum as function of applied bias (V_{ds} = V_{gs}) for organic light-emitting device using DPEPO:t-DABNA 10% blend. (inset) Main emission peak (*y*-left) and full width half maximum (right *y*-axis) as function of applied bias (V_{ds} = V_{gs}).

for practical OLET applications (beyond the scope of the present work).

Our study suggests that the incorporation of MR-TADF emitters into OLETs presents a promising route for further improvements in organic light-emitting transistors.

Conclusions

In this work we systematically investigated a multi-resonant TADF material, *t*-DABNA, embedded in DPEPO as a blue emissive layer in organic light-emitting transistors and we analysed our experimental results in terms of optical properties, morphological and optoelectronic properties of the blend itself. Optical characterization indicated that increasing the guest concentration resulted in a broadening of the main emission peak at lower energies. We found that emitter content of approximately 10% leads to the highest efficiency (EQE = 0.18%), independent of applied bias in the device and with a narrow band emission as low as 30 nm. These findings offer further insight into the potential of MR-TADF emitters such as *t*-DABNA in organic field-effect light-emitting devices, both on the importance of device engineering through concentration optimization as well as achieving narrowband emission.

Author contributions

G. F. conducted the experiments and characterization, analyzed the data and wrote the manuscript. A. A. supported through AFM studies and validation of device data. C. S. conceived and supervised the project. All authors contributed to the manuscript, provided feedback and approved the final version.

Conflicts of interest

There are no conflicts to declare.

Data availability

The data that support this publication are available within the article and its supplementary information (SI) or are available from the corresponding authors upon request. Supplementary information: schematic representation of TADF and MR-TADF Jablonski diagrams, absolute photoluminescence of DPEPO:*t*-DABNA blends on Si/SiO_2, external quantum efficiency as a function of gate voltage, CIE 1931 diagram of the electroluminescent OLETs, AFM image of C8-BTBT on PMMA. See DOI: https://doi.org/10.1039/d5ma01444a.

Acknowledgements

The authors acknowledge the support from the Research Council of Finland (WALLPAPER: grant no. 352914, TADF-Field: grant no. 355922 and PREIN Flagship Program grant no. 320167) and the use of MIDAS infrastructure of Aalto School of Electrical Engineering.

References

1 M. U. Chaudhry, K. Muhieddine, R. Wawrzinek, J. Sobus, K. Tandy, S. C. Lo and E. B. Namdas, *Adv. Funct. Mater.*, 2019, **30**, 1905282.
2 Z. Qin, H. Gao, J. Liu, K. Zhou, J. Li, Y. Dang, L. Huang, H. Deng, X. Zhang, H. Dong and W. Hu, *Adv. Mater.*, 2019, **31**, 1903175.
3 S. Z. Bisri, T. Takenobu, Y. Yomogida, H. Shimotani, T. Yamao, S. Hotta and Y. Iwasa, *Adv. Funct. Mater.*, 2009, **19**, 1728–1735.
4 F. Dinelli, R. Capelli, M. A. Loi, M. Murgia, M. Muccini, A. Facchetti and T. J. Marks, *Adv. Mater.*, 2006, **18**, 1416–1420.
5 C. F. Liu, X. Liu, W. Y. Lai and W. Huang, *Adv. Mater.*, 2018, **30**, 1802466.
6 A. Hepp, H. Heil, W. Weise, M. Ahles, R. Schmechel and H. von Seggern, *Phys. Rev. Lett.*, 2003, **91**, 157406.

7 L. Hou, X. Zhang, G. F. Cotella, G. Carnicella, M. Herder, B. M. Schmidt, M. Patzel, S. Hecht, F. Cacialli and P. Samori, *Nat. Nanotechnol.*, 2019, **14**, 347–353.
8 M. Xu, C. Zhao, Z. Meng, H. Yan, H. Chen, Z. Jiang, Z. Jiang, H. Chen, L. Meng, W. Hui, Z. Su, Y. Wang, Z. Wang, J. Wang, Y. Gao, Y. He and H. Meng, *Adv. Mater.*, 2023, **35**, 2307703.
9 Z. Qin, T. Wang, H. Gao, Y. Li, H. Dong and W. Hu, *Adv. Mater.*, 2023, **35**, 2301955.
10 Z. Xie, D. Liu, C. Gao, X. Zhang, H. Dong and W. Hu, *J. Am. Chem. Soc.*, 2025, **147**, 2239–2256.
11 J. Liu, H. Zhang, H. Dong, L. Meng, L. Jiang, L. Jiang, Y. Wang, J. Yu, Y. Sun, W. Hu and A. J. Heeger, *Nat. Commun.*, 2015, **6**, 10032.
12 E. B. L. Namdas, P. Ledochowitsch, J. D. Yuen, D. Moses and A. J. Heeger, *Appl. Phys. Lett.*, 2008, **92**, 183304.
13 H. Chen, W. Huang, T. J. Marks, A. Facchetti and H. Meng, *Small*, 2021, **17**, 2007661.
14 R. Capelli, S. Toffanin, G. Generali, H. Usta, A. Facchetti and M. Muccini, *Nat. Mater.*, 2010, **9**, 496–503.
15 J. Deng, W. Jia, Y. Chen, D. Liu, Y. Hu and Z. Xiong, *Sci. Rep.*, 2017, **7**, 44396.
16 S. Wu, M. Aonuma, Q. Zhang, S. Huang, T. Nakagawa, K. Kuwabara and C. Adachi, *J. Mater. Chem. C*, 2014, **2**, 421–424.
17 H. S. Kim, S.-R. Park and M. C. Suh, *J. Phys. Chem. C*, 2017, **121**, 13986–13997.
18 L. S. Cui, S. B. Ruan, F. Bencheikh, R. Nagata, L. Zhang, K. Inada, H. Nakanotani, L. S. Liao and C. Adachi, *Nat. Commun.*, 2017, **8**, 2250.
19 Y. Tao, C. Yang and J. Qin, *Chem. Soc. Rev.*, 2011, **40**, 2943–2970.
20 K. Zhang, J. Liu, Y. Zhang, J. Fan, C.-K. Wang and L. Lin, *J. Phys. Chem. C*, 2019, **123**, 24705–24713.
21 K. Gallegos-Rosas, P. Myllymäki, M. Saarniheimo, S. Sneck, R. Raju and C. Soldano, *ACS Appl. Electron. Mater.*, 2024, **6**, 1493–1503.
22 C. Soldano, O. Laouadi, V. Kornienko, K. Gallegos-Rosas and A. Azari, *ACS Photonics*, 2025, **12**, 5958–5969.
23 C. Soldano, O. Laouadi and K. Gallegos-Rosas, *ACS Omega*, 2022, **7**, 43719–43728.
24 A. Azari, G. Fanourakis, S. You, I. Concina and C. Soldano, *J. Mater. Chem. C*, 2025, **13**, 23028–23036.
25 M. Y. Wong and E. Zysman-Colman, *Adv. Mater.*, 2017, **29**, 1605444.
26 H. Uoyama, K. Goushi, K. Shizu, H. Nomura and C. Adachi, *Nature*, 2012, **492**, 234–238.
27 K. Goushi, K. Yoshida, K. Sato and C. Adachi, *Nat. Photonics*, 2012, **6**, 253–258.
28 T. J. Penfold, F. B. Dias and A. P. Monkman, *Chem. Commun.*, 2018, **54**, 3926–3935.
29 Y. Tao, K. Yuan, T. Chen, P. Xu, H. Li, R. Chen, C. Zheng, L. Zhang and W. Huang, *Adv. Mater.*, 2014, **26**, 7931–7958.
30 S. Huang, Q. Zhang, Y. Shiota, T. Nakagawa, K. Kuwabara, K. Yoshizawa and C. Adachi, *J. Chem. Theory Comput.*, 2013, **9**, 3872–3877.
31 H. Tanaka, K. Shizu, H. Miyazaki and C. Adachi, *Chem. Commun.*, 2012, **48**, 11392–11394.
32 A. Endo, K. Sato, K. Yoshimura, T. Kai, A. Kawada, H. Miyazaki and C. Adachi, *Appl. Phys. Lett.*, 2011, **98**, 083302.
33 H. Nakanotani, Y. Tsuchiya and C. Adachi, *Chem. Lett.*, 2021, **50**, 938–948.
34 D. Liu, J. De, H. Gao, S. Ma, Q. Ou, S. Li, Z. Qin, H. Dong, Q. Liao, B. Xu, Q. Peng, Z. Shuai, W. Tian, H. Fu, X. Zhang, Y. Zhen and W. Hu, *J. Am. Chem. Soc.*, 2020, **142**, 6332–6339.
35 Y. Huo, H. Qi, S. He, J. Li, S. Song, J. Lv, Y. Liu, L. Peng, S. Ying and S. Yan, *Aggregate*, 2023, **4**, 391.
36 X. Wu, S. Ni, C. H. Wang, W. Zhu and P. T. Chou, *Chem. Rev.*, 2025, **125**, 6685–6752.
37 K. R. Naveen, H. I. Yang and J. H. Kwon, *Commun. Chem.*, 2022, **5**, 149.
38 X. Wu, B.-K. Su, D.-G. Chen, D. Liu, C.-C. Wu, Z.-X. Huang, T.-C. Lin, C.-H. Wu, M. Zhu, E. Y. Li, W.-Y. Hung, W. Zhu and P.-T. Chou, *Nat. Photonics*, 2021, **15**, 780–786.
39 T. Hatakeyama, K. Shiren, K. Nakajima, S. Nomura, S. Nakatsuka, K. Kinoshita, J. Ni, Y. Ono and T. Ikuta, *Adv. Mater.*, 2016, **28**, 2777–2781.
40 X. F. Luo, X. Xiao and Y. X. Zheng, *Chem. Commun.*, 2024, **60**, 1089–1099.
41 J. Y. Wang, H. R. Zheng, X. Xiao and X. F. Luo, *Chem. Commun.*, 2025, **61**, 7434–7437.
42 H. Hirai, K. Nakajima, S. Nakatsuka, K. Shiren, J. Ni, S. Nomura, T. Ikuta and T. Hatakeyama, *Angew. Chem., Int. Ed.*, 2015, **54**, 13581–13585.
43 S. Madayanad Suresh, D. Hall, D. Beljonne, Y. Olivier and E. Zysman-Colman, *Adv. Funct. Mater.*, 2020, **30**, 1908677.
44 K. Stavrou, A. Danos, T. Hama, T. Hatakeyama and A. Monkman, *ACS Appl. Mater. Interfaces*, 2021, **13**, 8643–8655.
45 F. M. Winnik, *Chem. Rev.*, 1993, **93**, 587–614.
46 L. Xiaofeng, Z. Dongdong, D. Lian and Z. Yuewei, *Front. Chem.*, 2023, **11**, 1198404.
47 X. Liang, Z. P. Yan, H. B. Han, Z. G. Wu, Y. X. Zheng, H. Meng, J. L. Zuo and W. Huang, *Angew. Chem., Int. Ed.*, 2018, **57**, 11316–11320.
48 S. H. Han, J. H. Jeong, J. W. Yoo and J. Y. Lee, *J. Mater. Chem. C*, 2019, **7**, 3082–3089.
49 Z. Miao, C. Gao, M. Shen, P. Wang, H. Gao, J. Wei, J. Deng, D. Liu, Z. Qin, P. Wang, Y. Lei, S. C. Lo, X. Zhang, G. Yuan, E. B. Namdas, Y. Ma, H. Dong and W. Hu, *Nat. Mater.*, 2025, **24**, 917–924.
50 Z. Li, D. Liu and S.-J. Su, *Smart Mater. Devices*, 2025, **1**, 41402.
51 F. Huang, X. C. Fan, Y. C. Cheng, H. Wu, Y. Z. Shi, J. Yu, K. Wang, C. S. Lee and X. H. Zhang, *Mater. Horiz.*, 2022, **9**, 2226–2232.
52 K. Stavrou, L. G. Franca and A. P. Monkman, *ACS Appl. Electron. Mater.*, 2020, **2**, 2868–2881.
53 Q. Zhang, T. Komino, S. Huang, S. Matsunami, K. Goushi and C. Adachi, *Adv. Funct. Mater.*, 2012, **22**, 2327–2336.

54 J. H. Kim, W. J. Chung, J. Kim and J. Y. Lee, *Mater. Today Energy*, 2021, **21**, 100792.
55 K. H. Lee and J. Y. Lee, *Org. Electron.*, 2019, **75**, 105377.
56 J. Z. a H. Sirringhaus, *Chem. Rev.*, 2007, **107**, 1296–1323.
57 B. R. Masters, *Eur. Phys. J.*, 2013, **39**, 87–139.
58 J. Lee, N. Aizawa, M. Numata, C. Adachi and T. Yasuda, *Adv. Mater.*, 2017, **29**, 1604856.
59 Y. Kawamura, *Appl. Phys. Lett.*, 2008, **86**, 071104.
60 Z.-H. Lu, J.-X. Hu, Y.-N. Zhong, X. Zhou, C. Xu, X. Gao, J.-L. Xu, S. Duhm and S.-D. Wang, *Appl. Phys. Lett.*, 2018, **113**, 043302.
61 E. B. Namdas, B. B. Y. Hsu, Z. Liu, S. C. Lo, P. L. Burn and I. D. W. Samuel, *Adv. Mater.*, 2009, **21**, 4957–4961.
62 M. Ullah, R. Wawrzinek, R. C. R. Nagiri, S. C. Lo and E. B. Namdas, *Adv. Opt. Mater.*, 2017, **5**, 1600973.
63 H. Chen, M. Shi, M. Liu, X. Xing, C. Zhao, J. Miao, M. U. Ali, A. Facchetti and H. Meng, *ACS Appl. Mater. Interfaces*, 2020, **12**, 40558–40565.
64 M. Zambianchi, E. Benvenuti, C. Bettini, C. Zanardi, R. Seeber, D. Gentili, M. Cavallini, M. Muccini, V. Biondo, C. Soldano, G. Generali, S. Toffanin and M. Melucci, *J. Mater. Chem. C*, 2016, **4**, 9411–9417.